Supplementary Information: On charge percolation in slurry electrodes used in Vanadium Redox Flow Batteries

Johannes Lohaus[a,*], Deniz Rall[a,b,*], Maximilian Kruse[a], Viktoria Steinberger[a], Matthias Wessling[a,b,**]

[a]*RWTH Aachen University, AVT.CVT - Department of Chemical Engineering, Chemical Process Engineering, Forckenbeckstrasse 51, 52074 Aachen, Germany*
[b]*DWI - Leibniz Institute for Interactive Materials, Forckenbeckstrasse 50, 52074 Aachen, Germany*

1. Vanadium Redox Flow Battery

The general design of a VRB is illustrated in Figure 1. The cell is composed of two electrodes/current collectors and an ion-selective membrane as the separator. The membrane is placed in between the electrodes to form two half-cells. To maintain charge neutrality during the redox reaction, H^+ ions have to be transferred between the locations of the mixed reactions via the separator membrane. The (ideal) membrane should have a high permeability for protons. Contrary to non-flowing cells, the electrolyte is stored in two external tanks that are coupled to separate fluid circuits. Within these circuits, the electrolyte is pumped through the half-cells where the actual charge/discharge mechanisms occur. Thus a potential between the electrodes of the cell either has to be applied externally (charging) or can be tapped (discharging) [1].

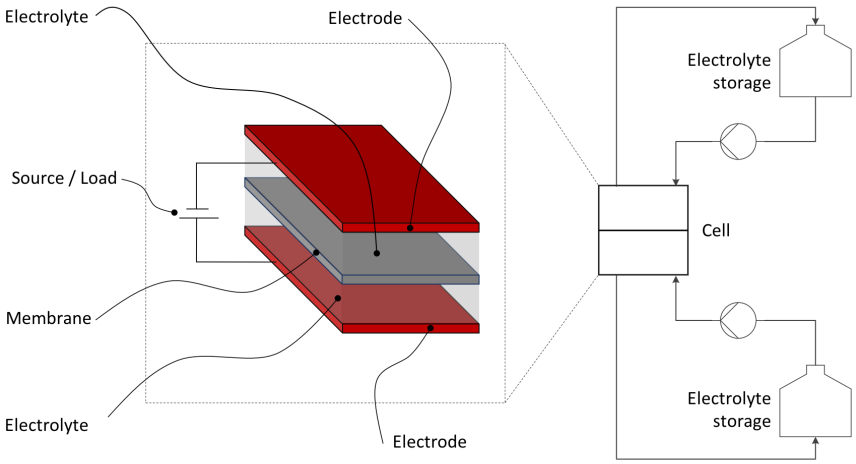

Figure 1: Design of an All-Vanadium Redox Flow Battery

*These authors contributed equally to this work
**Corresponding author: manuscripts.cvt@avt.rwth-aachen.de

2. CFD DEM modeling

This study uses the CFDEM ® framework, which combines OpenFoam ® and LIGGGHTS ®. The volume-averaged Navier-Stokes equations determines the flow of the fluid phase [2, 3]:

$$\frac{\partial \alpha_f}{\partial t} + \nabla \cdot (\alpha_f u_f) = 0 \tag{1}$$

$$\frac{\partial \alpha_f u_f}{\partial t} + \nabla \cdot (\alpha_f u_f u_f) = -\alpha_f \nabla \frac{p}{\rho_f} - R_{pf} + \nabla \cdot \tau \tag{2}$$

p and u_f are the pressure and the velocity of the fluid phase. α_f is the local volume fraction of the fluid within the suspension and $\tau = \nu_f \nabla u_f$ its stress tensor. R_{pf} is a source term to consider the momentum exchange between the liquid and the solid phase. This quantity arises from velocity differences between the phases and primarily causes a drag force on the particles. Under the assumption of a drag force dominance, the momentum exchange can be calculated as [2]:

$$R_{pf} = K_{pf}(u_f - u_p) \tag{3}$$

$$K_{pf} = \begin{cases} \frac{3}{4} C_d \frac{\alpha_f (1-\alpha_f) u_f - u_p}{d_p} \alpha_f^{-2.65}, & \alpha_f > 0.8 \\ 150 \frac{(1-\alpha_f)^2 \nu_f}{\alpha_f d_p^2} + 1.75 \frac{(1-\alpha_f) u_f - u_p}{d_p}, & \alpha_f \leqslant 0.8 \end{cases} \tag{4}$$

Furthermore it is:

$$C_d = \frac{24}{\alpha_f Re_p} \left[1 + 0.15 (\alpha_f Re_p)^{0.687} \right] \tag{5}$$

$$Re_p = \frac{u_f - u_p}{\nu_f} d_p \tag{6}$$

where u_p is the particle velocity, d_p its diameter. Re_p, K_{pf} and C_d donate the particle Reynolds number, the momentum exchange coefficient and the drag coefficient, respectively. Generally the trajectory of a distinct particle is calculated from Newton's law and the principle of angular momentum [2]:

$$m\,\ddot{x} = F_n + F_t + F_b + F_f \tag{7}$$

$$I \frac{d\omega}{dt} = r \times F_t + T_r \tag{8}$$

Thereby m and $\ddot{x}$ refer to the particle mass and acceleration, respectively. The forces acting on the particle can be subdivided into the mechanical contact forces F_n (normal) and F_t (tangential), the fluid force F_f and the sum of other body forces F_B. The latter comprises e.g. Van der Waals interactions. Regarding the equation for the angular velocity, r is the radius and T_r an additional momentum due to rolling friction [2–4].

The contact forces F_n (normal) and F_t (tangential) are approximated by a spring-dashpot-model. Thereby, the model bases on non physical interpenetrations of contacting surfaces. The normal contact force is calculated as following:

$$F_n = -k_n \delta_n + c_n \delta u_n \tag{9}$$

where δ_n is the normal overlap and δu_n the velocity difference of the intersecting surfaces. In addition, k_n is the normal spring coefficient and c_n the damper coefficient.

These coefficients are derived from the mechanical properties of the intersecting bodies [2, 5, 6]:

$$k_n = \frac{4}{3} Y^* \sqrt{R^* \delta_n} \tag{10}$$

$$c_n = -2 \sqrt{\frac{5}{6}} \beta \sqrt{S_n m^*} \tag{11}$$

with:

$$S_n = 2Y^* \sqrt{R * \delta_n} \tag{12}$$

$$\beta = \frac{ln(e_r)}{ln^2(e_r) + \pi^2} \tag{13}$$

$$\frac{1}{Y^*} = \frac{1 - \nu_1^2}{Y_1} + \frac{1 - \nu_2^2}{Y_2} \tag{14}$$

$$\frac{1}{R^*} = \frac{1}{R_{p,1}} + \frac{1}{R_{p,2}}, \quad \frac{1}{m^*} = \frac{1}{m_1} + \frac{1}{m_2} \tag{15}$$

Here R_p denotes the particles' radius, m their mass, Y the Young's modulus, ν the Poisson ratio and e_r the coefficient of restitution.

Moreover, the tangential contact force is calculated in a similar way:

$$F_t = min\left\{ \left[k_t \int_{t_{c,0}}^{t} \Delta u_t dt + c_t \Delta u_t \right], \mu F_n \right\} \tag{16}$$

It should be noted that the tangential spring deflection is calculated from the temporal integral of the intersecting bodies' tangential velocity difference. Again, the spring and damper coefficients are calculated from mechanical properties [2, 5, 6]:

$$k_t = 8 G_S^* \sqrt{R^* \delta_n} \tag{17}$$

$$c_t = -2 \sqrt{\frac{5}{6}} \beta \sqrt{S_t m^*} \tag{18}$$

with:

$$S_t = 8 G_S^* \sqrt{R * \delta_n} \tag{19}$$

$$\frac{1}{G_S^*} = \frac{2(2 - \nu_1)(1 + \nu_1)}{Y_1} + \frac{2(2 - \nu_2)(1 + \nu_2)}{Y_2} \tag{20}$$

where G_S is the shear modulus.

In addition to the contact mechanics, the modeling approach incorporates colloidal interactions namely the DLVO theory. The DLVO theory combines the van der Waals and double layer potential. Since VRFB work at high electrolyte concentrations ($> 1M$) the double layer interactions can be neglected due to charge screening.

The van der Waals potential determined by Hamaker [7] between two spheres (S) with radii a whose surfaces are separated by the distance D is given by

$$W_{\mathrm{VDW}}^{\mathrm{SS}}(D) = -\frac{A}{6}\left\{\frac{2a^2}{D(4a+D)} + \frac{2a^2}{(2a+D)^2} + \ln\frac{D(4a+D)}{(2a+D)^2}\right\} \tag{21}$$

and for a sphere and an infinite flat plate (P) by

$$W_{\mathrm{VDW}}^{\mathrm{SP}}(D) = -\frac{A}{6}\left\{\frac{a}{D} + \frac{a}{D+2a} + \ln\frac{D}{D+2a}\right\}. \tag{22}$$

One can compute the force acting on a sphere in such a potential field using the relation

$$\boldsymbol{F}(D) = -\nabla W(D), \tag{23}$$

where ∇ denotes the spatial gradient.

3. Work flow of the simulation model

Summarized, Figure 2 shows the working flow of the simulation model indicating the path of the coupling scheme.

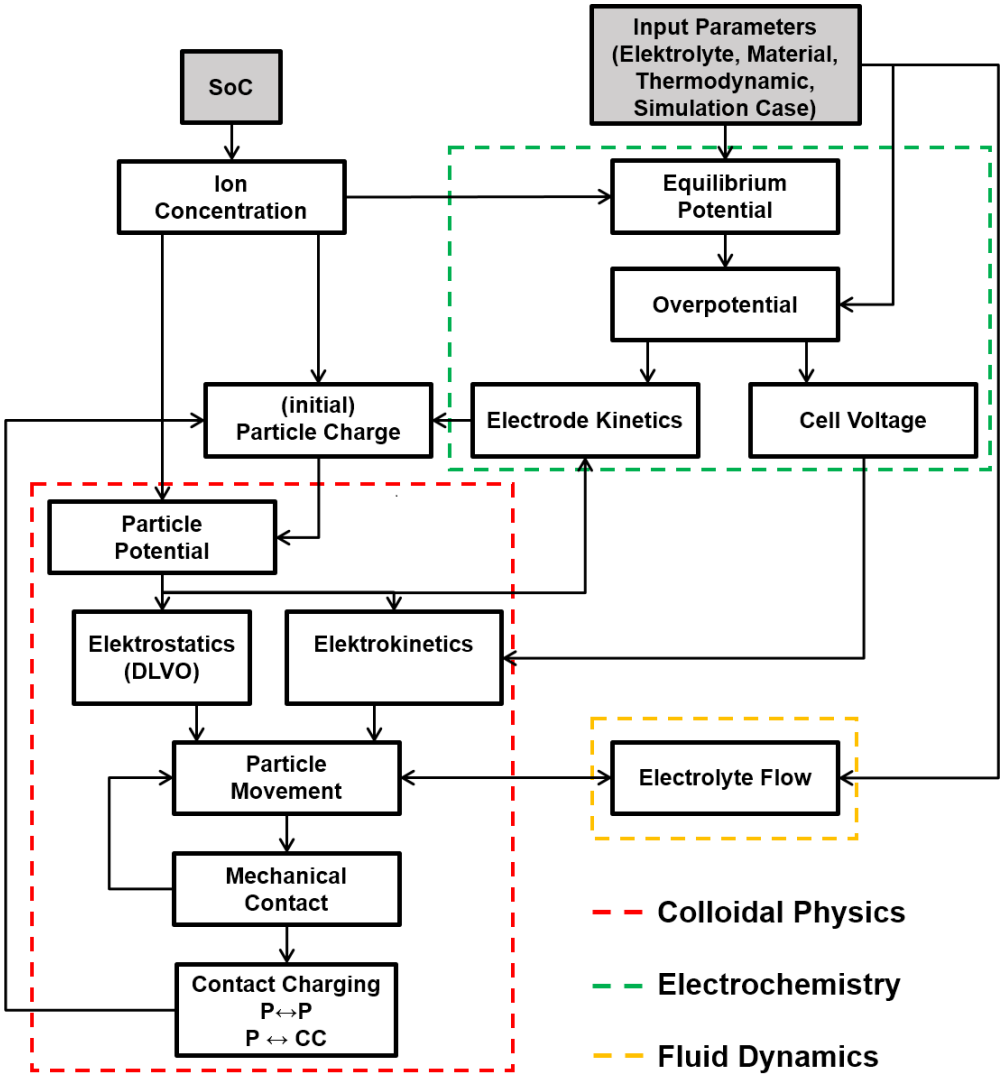

Figure 2: Program structure for the coupled fluid particle simulation

4. Electrochemistry in the battery cell

The charge transfer takes place during contact of particles with the current collector or among one another. An instant charge transfer is assumed. By contact between a particle with the current collector, we assume the particle adopts the potential of the current collector. In the case of a particle-particle contact a charge balancing model is applied, where both particles adopt the arithmetic average of their potentials before contact. The kinetics of charge distribution in a material has to be considered qualitatively to assess the reasonableness of this concept. They can be characterized by the so-called charge relaxation time. The relaxation time denotes the period a system requires to reach equilibrium after a deviation from the latter. Concerning charge relaxation, this is the duration of the compensation of electric potential gradients within the material in accordance with Gauss's law [8]. For conductors, this time is of the order of 10^{-17} to 10^{-19} seconds [9]. On the contrary, the contact duration has to be evaluated as the amount of time available for the charge transfer. It can be derived from the Hertz model [5, 6]:

$$t_c = 2.87\Big[\frac{m^{*2}}{R^* y^{*2} v_{max}}\Big]^{0.2} \tag{24}$$

Here, v_{max} is the maximum normal velocity difference during contact.The effective quantities m^*, R^* and E^* donate the equivalent mass, radius and the Young's modulus of two contacting bodies [10]. For typical values, the Hertzian contact time is in the order of 10^{-5} to 10^{-8} seconds. Consequently, the kinetics of the charge transfer are fast compared to the duration of the contact and their neglect, which agrees with literature findings [11].

The conductive particles store electric charge in the electrostatic double layer. The electrostatic double layer base on the assumption that the excess charge of a surface in a liquid is compensated by counter ions bound to the surface as well as form a diffusive layer around the surface (Gouy-Chapman-Stern Theory) [12–14]. The electric charge stored in the double layer contains a rigid part with capacitor-like behavior, also called the Stern or Helmholtz layer, followed by a diffusive part obeying the laws of the Poisson-Boltzmann theory.

For higher electrolyte concentrations as they occur in a VRB, the counterions are compressed to the particle surface. The counter ions mainly bound rigidly onto the surface. This phenomenon is confirmed by the development of the double layer capacity [12, 13]. Therefore, equation 25 derived from the model of the parallel plate capacitor [12, 13, 15]:

$$\sigma = \frac{\epsilon_r \epsilon_0}{d_{HH}} \psi \tag{25}$$

is used to determine the correlation between charge and potential of the particles. Here, σ is the charge density of the considered body, ϵ_r, ϵ_0 are the relative permittivity of the surrounding medium and the electric constant and ψ signs for the potential. The size of the Stern layer d_{HH} depends on the electrolyte concentration and can be up to the size of several radii of the involved molecular species [16, 17]. For the description of the kinetics of the electrochemical conversion can be derived from the theory of homogeneous reactions. The reaction kinetic in the electrochemical cell is described by the modified Butler Vollmer equation:

$$i = A_s F k c_{II}^{\alpha_c} c_{III}^{\alpha_a} \left[\frac{c_{III}^S}{c_{III}} exp\Big(- \frac{\alpha_c F \eta}{RT} \Big) - \frac{c_{II}^S}{c_{II}} exp\Big(\frac{\alpha_a F \eta}{RT} \Big) \right] \tag{26}$$

where the Roman indices stand for the equivalent vanadium species and the exponent S denotes their concentration at the electrode surface. Moreover, the overpotential η means the potential difference between the inner electrode surface and the electrolyte concentration at its outer surface, which is non-zero due to excess concentration of ions. As simplification we assumed that the mass transfer of Va ions is much faster than the reaction kinetics leading to $\frac{c_i^S}{c_i} = 1$. This is valid if we assume that the redox reaction only occurs at the particles surface. If we further assume only diffusive transport to the particle surface, we can apply a Sherwood correlation for the mass transfer to our model. In simulations, we do not observe any mass transfer limitations. However, we do not consider redox reactions in the porous structure of the particle. In this case, mass transfer limitations may play a significant role because the diffusion path increases.

5. Simulation settings

Parameter	Symbol	Value	Unit
Flow velocity	u	1	$\mathrm{mm\,s^{-1}}$
Particle radius	a	10	µm
Young modulus	E	1×10^8	Pa
Poisson ratio	$\tilde{\nu}$	0.45	-
Coefficient of restitution	e	0.85	-
Friction coefficient	μ_f	0.5	-
Particle density	ρ_P	1000	$\mathrm{kg\,m^{-3}}$
Particle volume fraction	$V_\mathrm{P,fraction}$	$10 - 35$	vol %
Vanadium concentration	c_V	2.8	$\mathrm{mol\,L^{-1}}$
Permittivity of electrolyte solution	ϵ_r	90	
Anodic transfer coefficient	α_a	0.5	-
Cathodic transfer coefficient	α_c	0.5	-
Active surface	A_s	1.4	$\mathrm{m^2\,g^{-1}}$
Size of Stern layer	d_{hh}	0.1	nm
Overpotential	η	-0.1	V
Standard rate constant	k	1.7×10^{-7}	$\mathrm{m\,s^{-1}}$
Hamaker constant	A	1.4×10^{-20}	J
DEM-time step	Δt_DEM	1.0×10^{-8}	s
CFD-time step	Δt_CFD	1.0×10^{-6}	s

Table 1: Parameters applied in the simulation

[1] M. Skyllas-Kazacos, M. Rychcik, R.G. Robins, A.G. Fane, and M.A. Green. New all-vanadium redox flow cell. Journal of the Electrochemical Society, 133:1057, 1986.
[2] C. Kloss, C. Goniva, A. Hager, S. Amberger, and S. Pirker. Models, algorithms and validation for opensource DEM and CFD-DEM. Progress in Computational Fluid Dynamics, An International Journal, 12(2/3):140–152, 2012.
[3] C. Goniva, C. Kloss, A. Hager, and S. Pirker. An open source cfd-dem perspective. In Proceedings of OpenFOAM Workshop, Göteborg, pages 1–10, 2010.
[4] H.R. Norouzi, R. Zarghami, R. Sotudeh-Gharebagh, and N. Mostoufi. Coupled CFD-DEM modeling: Formulation, Implementation and Application to Multiphase Flows. John Wiley & Sons, 2016.
[5] C. Kloss. LIGGGHTS(R)-PUBLIC documentation, 2010.
[6] A. Di Renzo and F.P. Di Maio. Comparison of contact-force models for the simulation of collisions in DEM-based granular flow codes. Chemical Engineering Science, 59(3):525–541, 2004.
[7] H.C. Hamaker. The londonvan der waals attraction between spherical particles. Physica, 4(10):1058–1072, 1937.
[8] A.J. Bard. Electrochemical Dictionary. Springer, Berlin, 2008.
[9] S. Rennecke and A. P. Weber. Charge transfer to metal nanoparticles bouncing from conductive surfaces. Aerosol Science and Technology, 48(10):1059–1069, 2014.
[10] A. Di Renzo and F.P. Di Maio. An improved integral non-linear model for the contact of particles in distinct element simulations. Chemical engineering science, 60(5):1303–1312, 2005.
[11] W. John. Particle-surface interactions: Charge transfer, energy loss, resuspension, and deagglomeration. Aerosol Science and Technology, 23(1):2–24, 1995.
[12] W. Vielstich and C.H. Hamann. Elektrochemie. Wiley-VCH Verlag, Weinheim, 4th ed. edition, 2005.
[13] A.J. Bard and L.R. Faulkner. Electrochemical Methods: Fundamentals and Applications. Wiley-Interscience, New York and London, 2nd ed. edition, 2000.
[14] O. Stern. Zur Theorie der elektrolytischen Doppelschicht. Zeitschrift für Elektrochemie und angewandte physikalische Chemie, 30(21-22):508–516, 1924.
[15] H. von Helmholtz. Studien über electrische Grenzschichten. Annalen der Physik, 243(7):337–382, 1879.
[16] R. D. Shannon. Revised effective ionic radii and systematic studies of interatomic distances in halides and chalcogenides. Acta Crystallographica Section A, 32(5):751–767, 1976.
[17] J. F. Mcclendon. On the thickness of the helmholtz double layer. Science, 66(1704):200, 1927.